Supplementary Information for

Subsurface Architecture of the Tuina Prospect and Its Relationship to Fluid Migration in Mineral Deposit Formation

Javiera Jaque-Reyes[1,2], Valentina Reyes-Wagner[1,*], Diana Comte[1,2], Matías Peña[1], Daniela Calle-Gardella[1], Sergio Leon-Rios[1], Steven W. Roecker[3], Felipe Jiménez[4] and Sergio Pichott[5]

[1] Advanced Mining Technology Center, Universidad de Chile, 8370451, Santiago, Chile

[2] Departamento de Geofísica, Facultad Ciencias Físicas y Matemáticas, Universidad de Chile, 8370449, Santiago, Chile

[3] Earth and Environmental Sciences, School of Science, Rensselaer Polytechnic Institute, Troy, NY, 12180, USA

[4] Exploraciones Mineras S.A. EMSA-CODELCO, Av. Vitacura 2670, Santiago, Chile

[5] CODELCO, Gerencia de Exploraciones, Casa Matriz, Huérfanos 1270, Santiago, Chile

*Corresponding author: valentina.reyes-wagner@amtc.uchile.cl

List of contents:

Figure S1 - Wadati diagram

Figure S2 - Seismicity distribution

Figure S3 - Hypocenter uncertainties and arrival-times residuals, refined seismic catalog

Figure S4 - Hypocenter misfits from synthetic tests

Figure S5 - Standard checkerboard test for Vp and Vs, mapview

Figure S6 - Standard checkerboard test for Vp and Vs, section view

Figure S7 - Standard checkerboard test for Vp/Vs

Figure S8 - Seismic velocity model for P-wave (Vp), map views

Figure S9 - Seismic velocity model for P-wave, map and section views

Figure S10 - Vp and Vp/Vs model, comparison with regional model

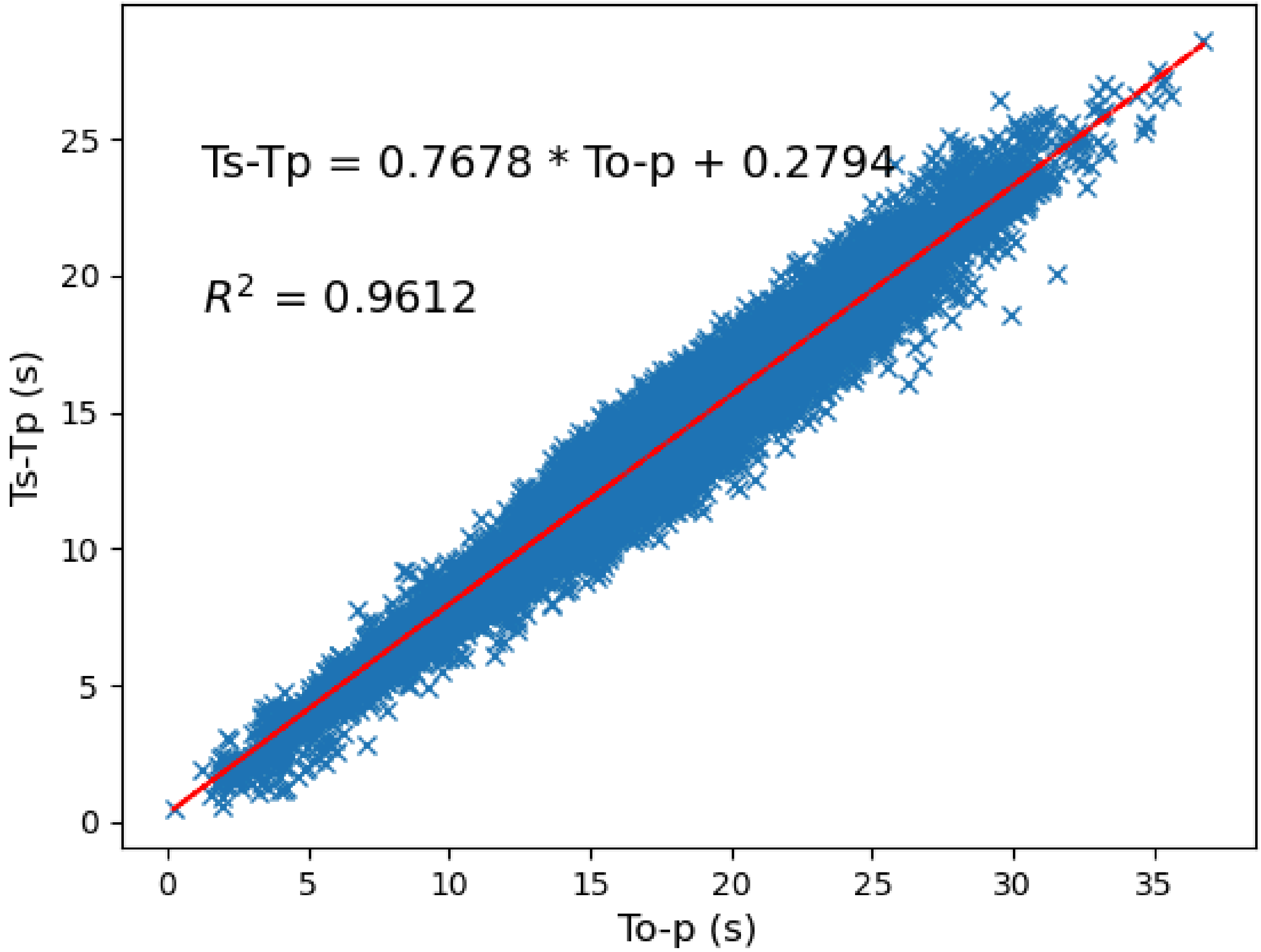

Figure S1. Wadati diagram to determine the initial Vp/Vs ratio for the inversion. The catalog with the arrival times was filtered based on the number of phases identified for each event: for shallow earthquakes (<20 km), a minimum of 8 phases was established for the P-wave, and 6 for the S-wave, while for deep earthquakes (>20 km), a minimum of 15 and 10 phases were needed, respectively. In both cases, earthquakes with three times more P-wave than S-wave arrivals were filtered out. The difference between P- and S-wave, $ts - tp$, was calculated and plotted against $t0 - tp$. The slope value is associated with the Vp/Vs, which in our study is 1.77.

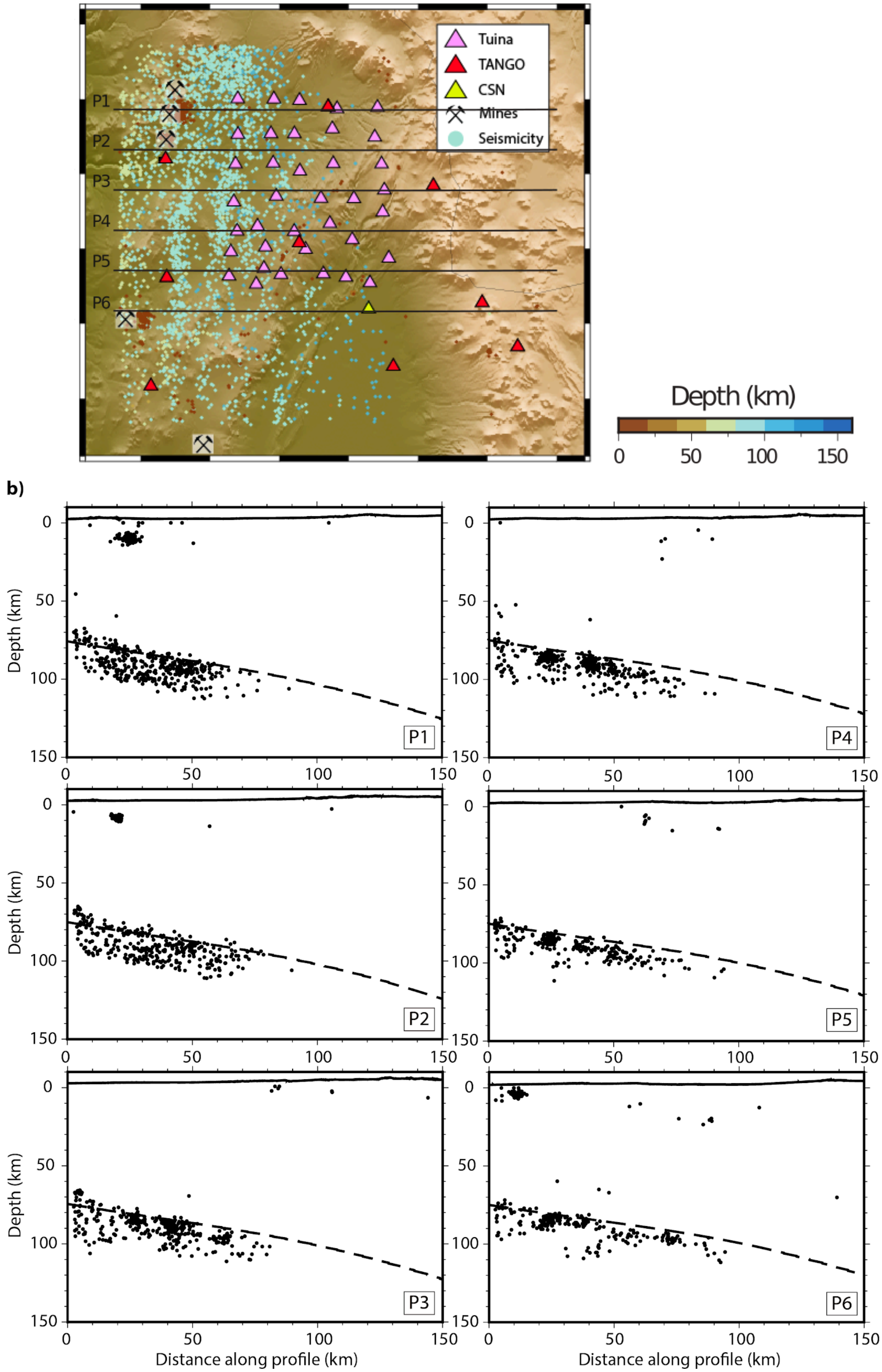

Figure S2: Earthquake locations from the refined catalog. **a)** Map view. Seismicity distribution colored by event depth. Triangles represent the seismic stations used in this study. Digital elevation model (DEM) derived from SRTM data. **b)** Section views with seismicity projected along profiles 10 km wide.

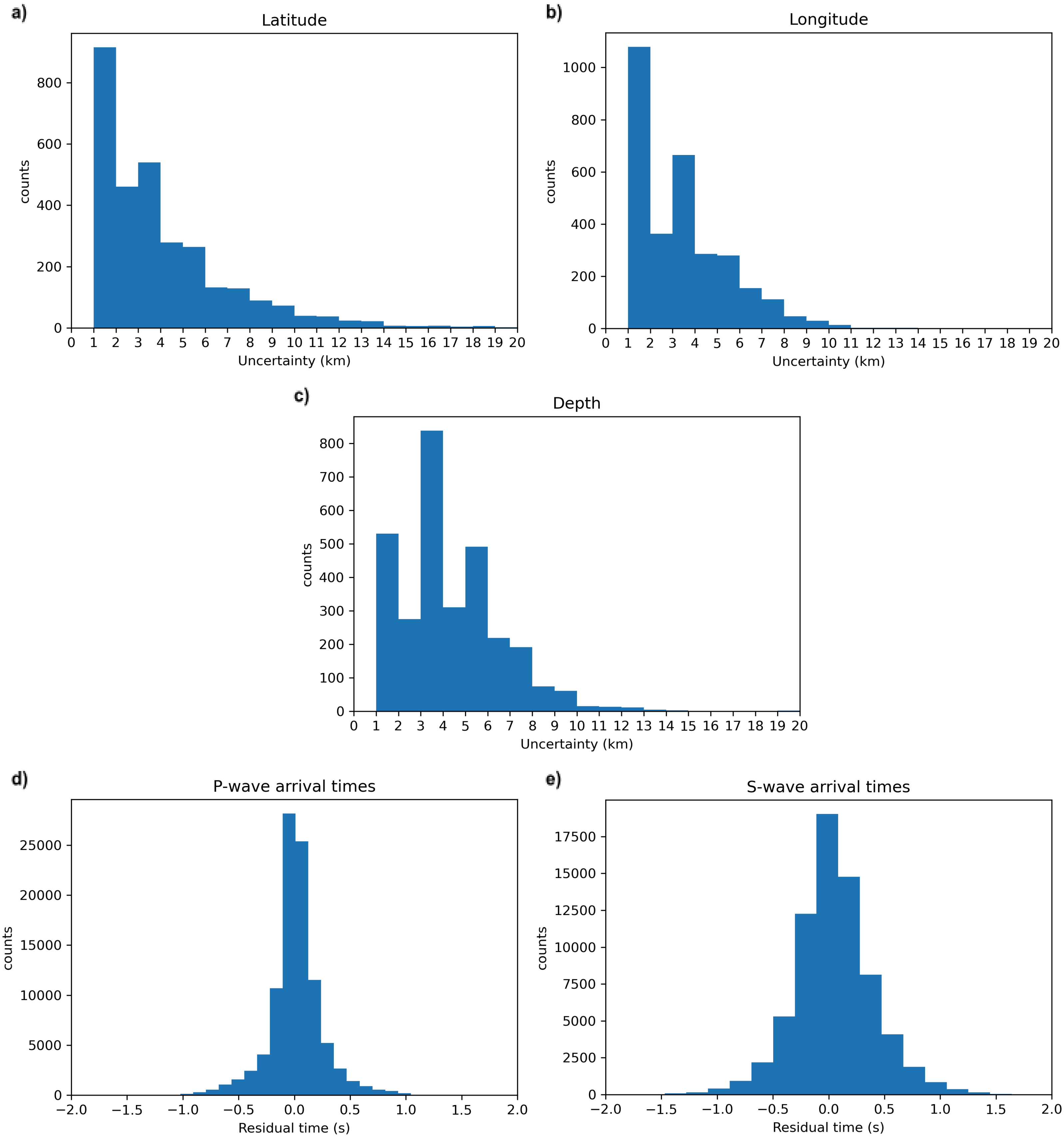

Figure S3. Statistics for the refined catalog. Uncertainties of the hypocenters in **a)** latitude, **b)** longitude, and **c)** depth in km. Residual times for **d)** P-wave and **e)** S-wave arrival times.

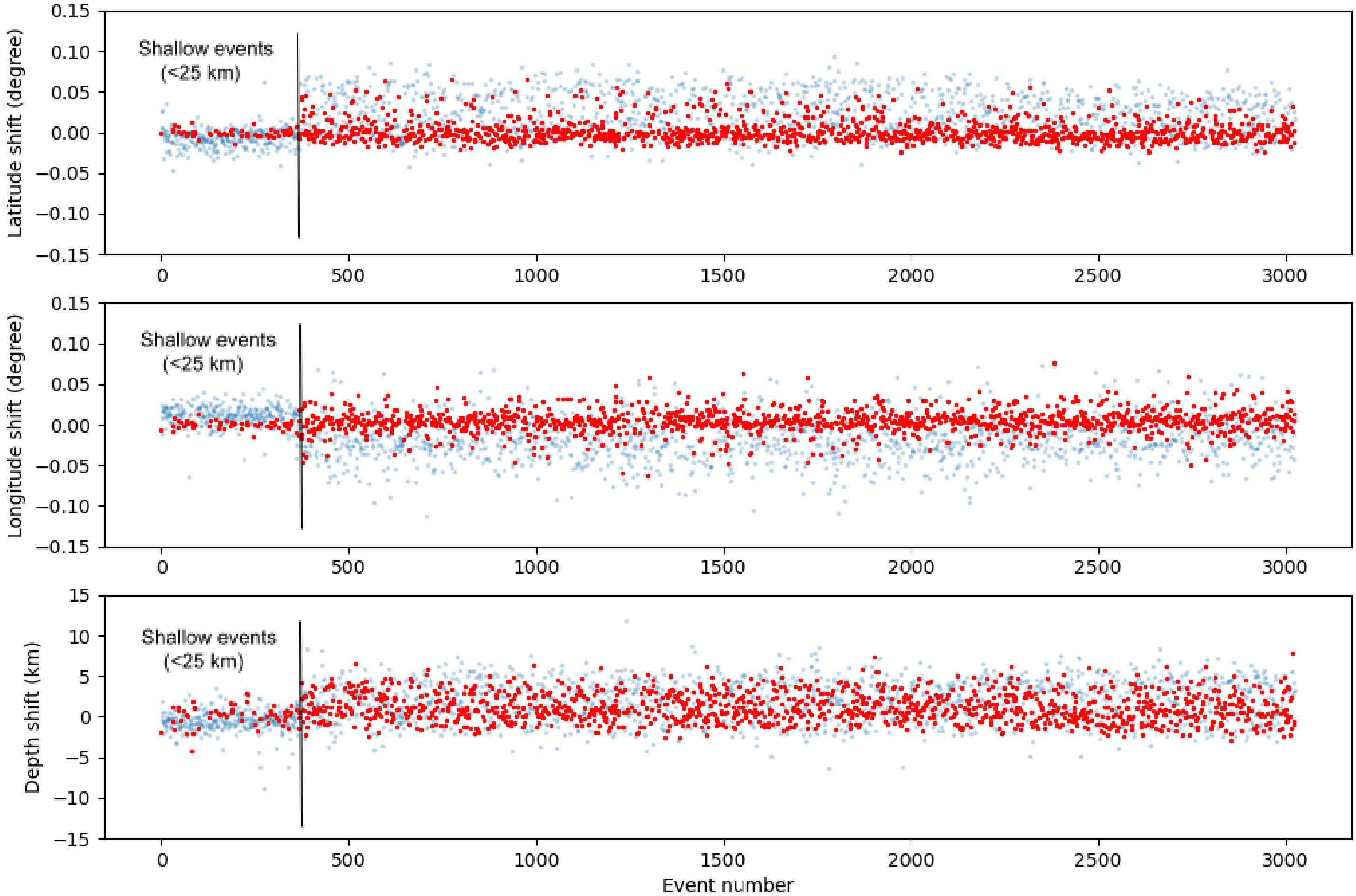

Figure S4. Hypocenter misfits from synthetic tests. Blue dots show the complete catalog and red dots the events that lie inside our network aperture. The synthetic catalog was generated by perturbing the refined real-event locations by up to 0.05° in latitude and longitude, and up to 5 km in depth. Synthetic arrival times were computed using the final velocity model. The inversion was performed using the same station geometry and inversion parameters as in the real-data processing. The plot shows the differences between true (synthetic) and recovered hypocenter locations in the horizontal and vertical components. The average latitude, longitude, and vertical misfits are 0.018°, 0.018°, and 2 km, respectively.

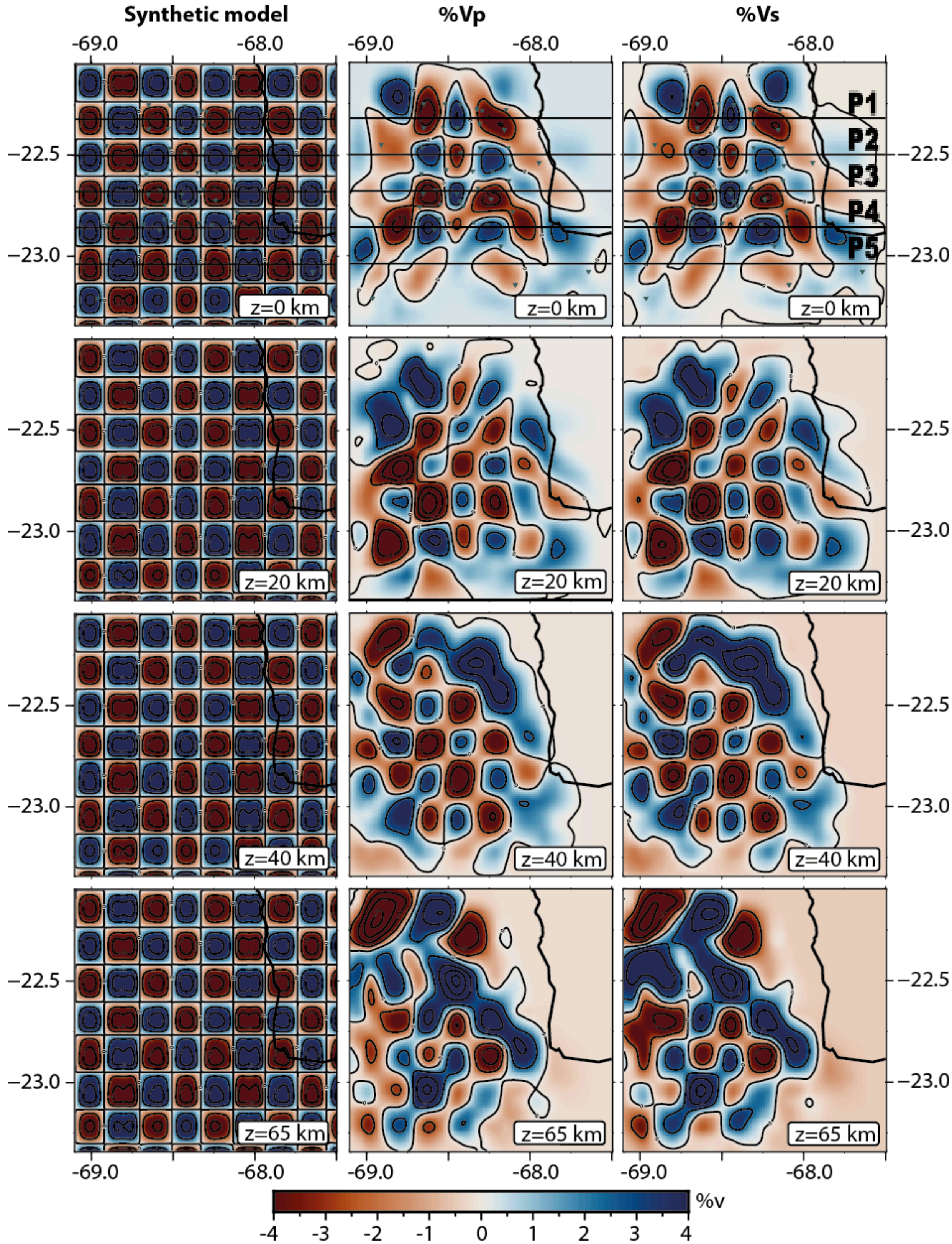

Figure S5. Standard checkerboard test of synthetic squared anomalies of 15 km size (left) for Vp (center) and Vs (right) presented in mapview. Horizontal slices at z= 0 km, 20 km, 40 km, and 65 km are shown. The checkerboard model is formed by alternating positive and negative perturbations of ±5% of the initial velocities. The data was perturbed by adding random Gaussian noise. Vp and Vs panels show the recovered velocities at the mentioned depths.

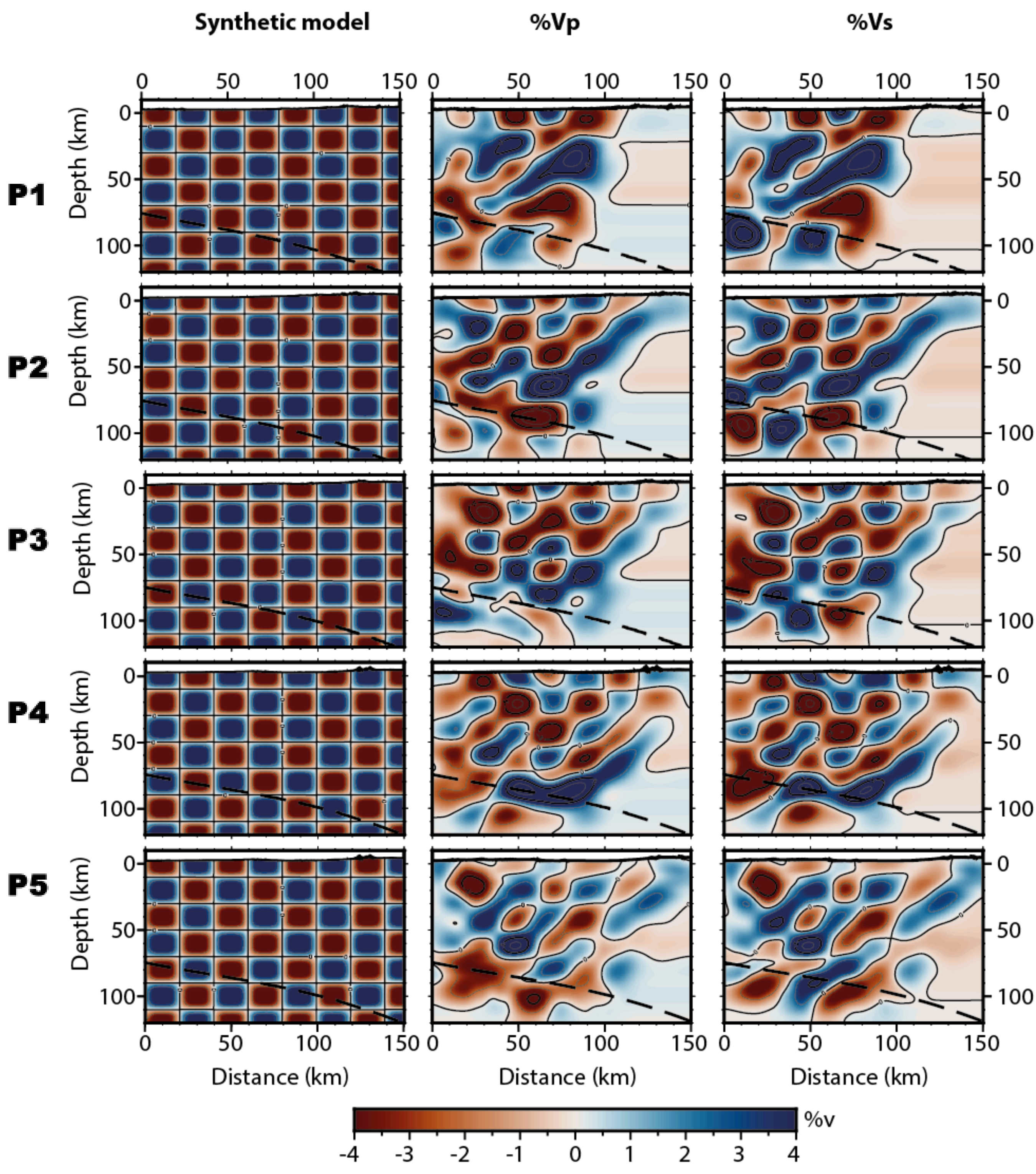

Figure S6. Standard checkerboard test of synthetic squared anomalies of 15 km size (left) for Vp (center) and Vs (right) presented in section view. Left panels show the initial checkerboard model with alternate positive and negative perturbations of ±5% of the velocities. The data was perturbed by adding random Gaussian noise. Central and right panels show the recovered velocities for Vp and Vs, respectively, along four representative profiles. The segmented black line shows the slab 2.0 model from Hayes et al. (2018).

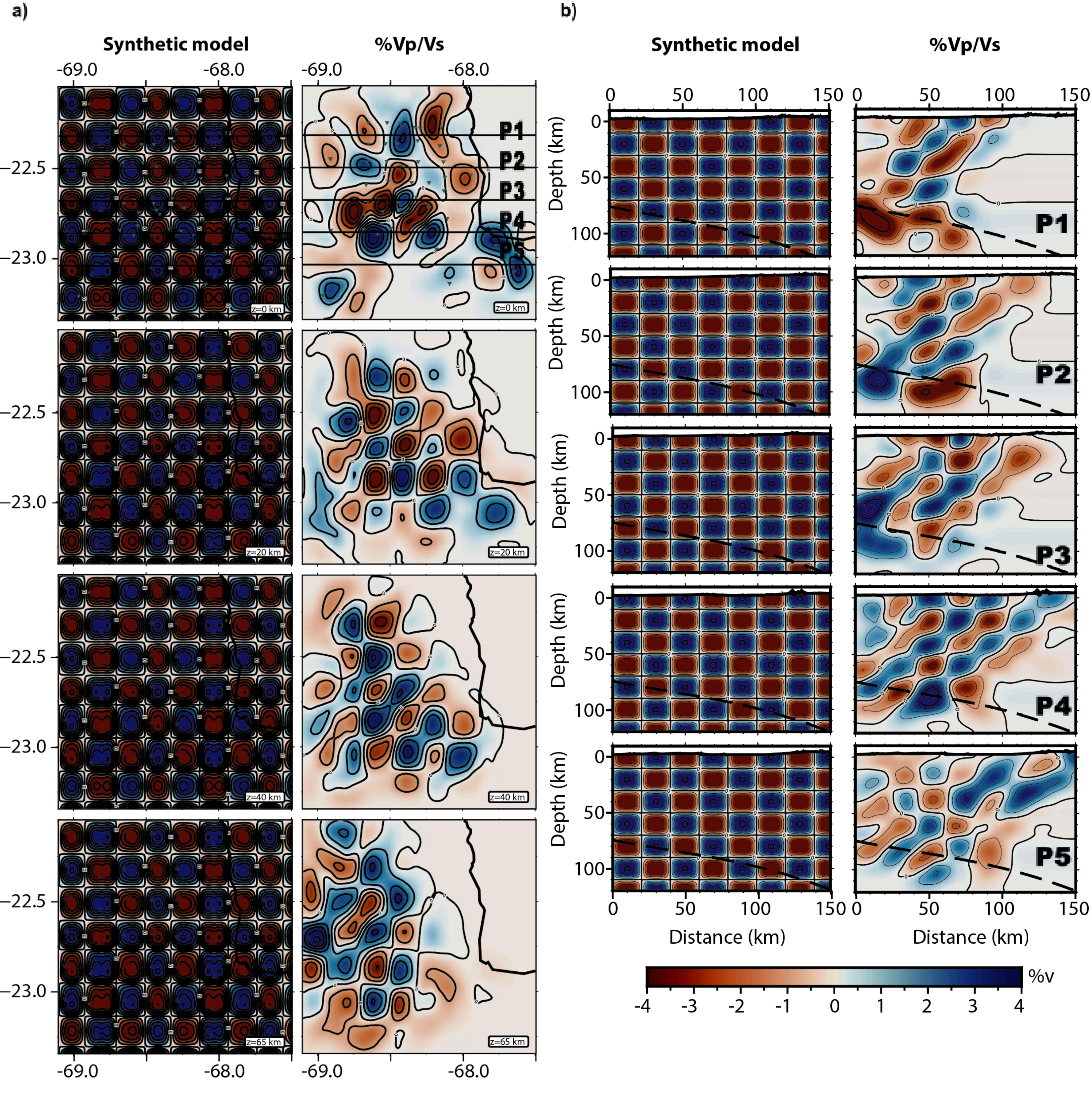

Figure S7. Standard checkerboard test of synthetic squared anomalies of 15 km size for Vp/Vs presented in **a)** map view and **b)** section view. Left panels show the initial checkerboard model with alternate positive and negative perturbations of ±5% of the velocities, achieved by perturbing Vp and Vs models by 2.5% each with opposite signs. The data was perturbed by adding random Gaussian noise. The left panels show the recovered velocities for Vp/Vs. Segmented black line shows the slab 2.0 model from Hayes et al., (2018).

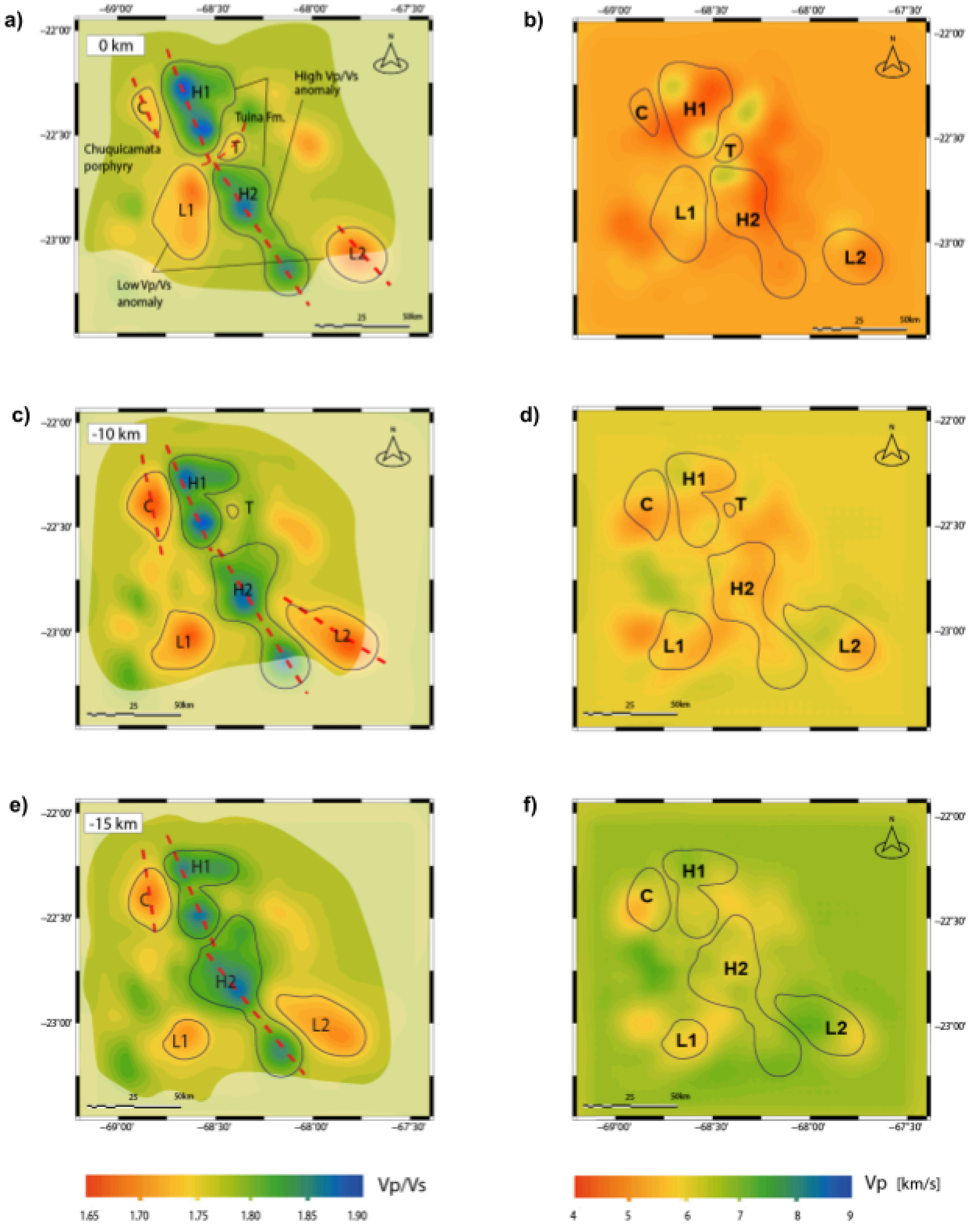

Figure S8. Seismic velocity models determined in this work in map views for Vp/Vs (left) and Vp (right) at different depths: **a)** and **b)** at sea level, **c)** and **d)** at 10 km depth; and **e)** and **f)** at 15 km depth. Anomalies T, C, L1, L2, H1, and H2 are delineated with red segmented lines showing their orientation.

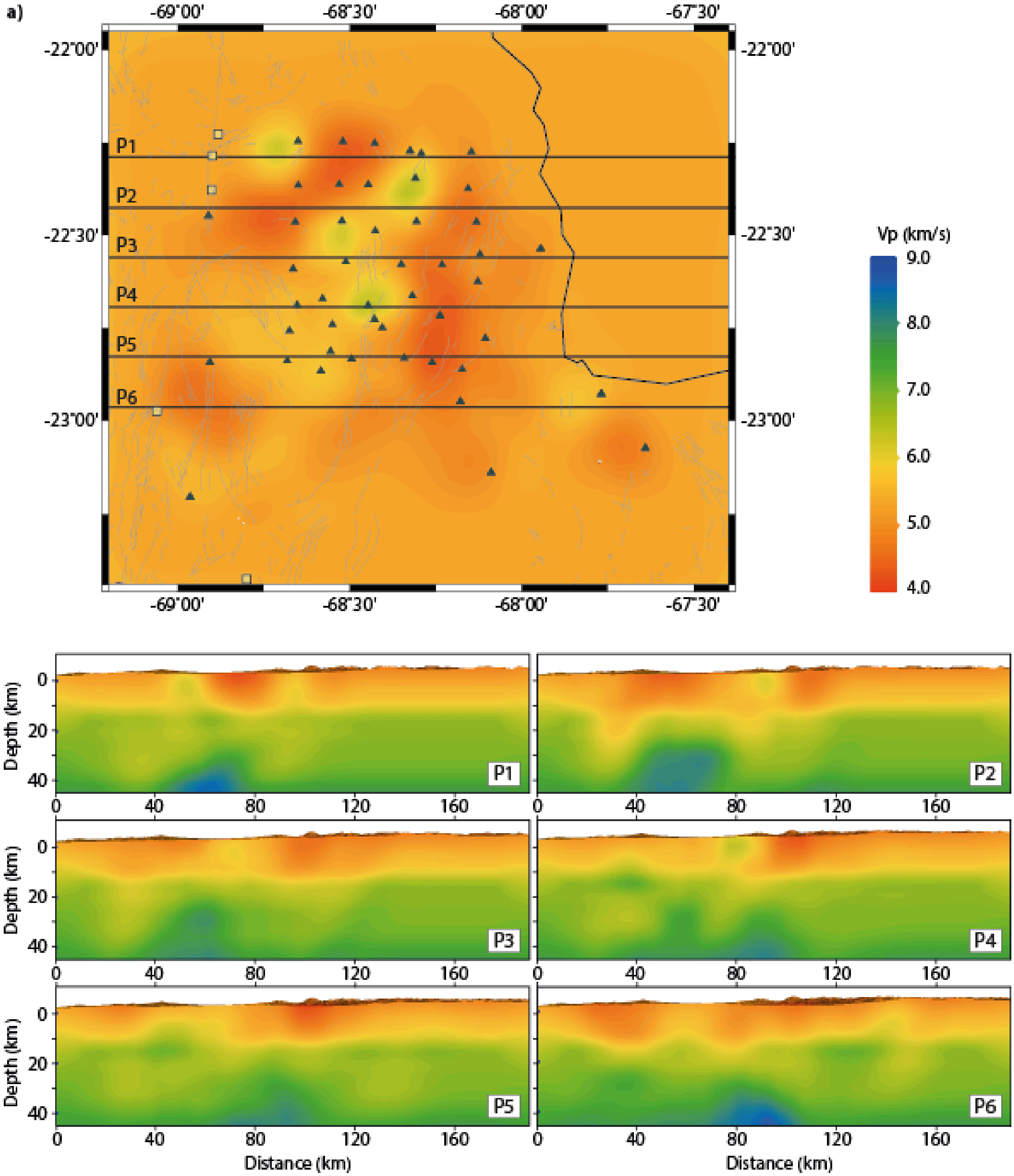

Figure S9. Seismic velocity model for P-wave (Vp) determined in this work, presented in mapview at sea level (top) and section profiles (bottom).

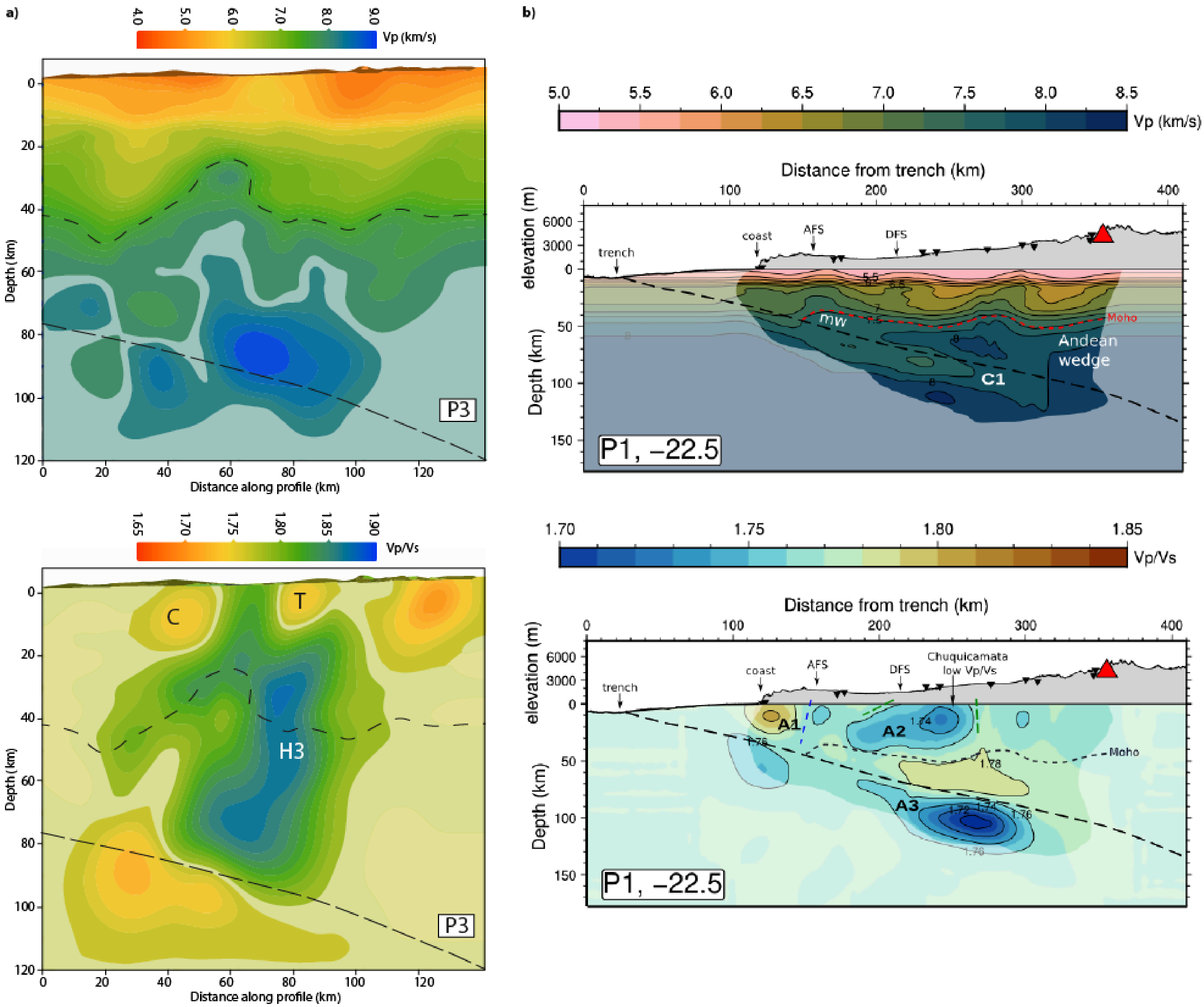

Figure S10. Comparison between **a)** Vp and Vp/Vs models determined in this work and **b)** Vp and Vp/Vs models from León-Ríos et al. (2024), at similar latitudes. Note that color-codes are inverted for the figures in Leon-Rios et al.